EIEC 2025

XVI Iberian Meeting on Computational Electromagnetics
Aveiro, Portugal / May 6-9, 2025

BOOK OF ABSTRACTS

ANACOM AUTORIDADE NACIONAL DE COMUNICAÇÕES

CT CADTECH

it instituto de telecomunicações

ORDEM DOS ENGENHEIROS TÉCNICOS PORTUGAL

ROHDE&SCHWARZ

universidade de aveiro

XVI EIEC

16th Iberian Meeting on Computational Electromagnetics

Session 2D

Thursday afternoon, 8th May, 17:00-18:20

Antennas and filters

Chair: Rafael Boix

Time	Title	Authors	Affiliation
17:00-17:20	On the use of filters for microstrip antenna design	I. M. Delgado-Lozano A. Fernández-Prieto V. Losada R. R. Boix	Microwave Group, Dept. of Electronics and Electromagnetism, College of Physics, Seville; Microwave Group, Dept. of Applied Physics I, School of Computer Engineering, Seville.
17:20-17:40	Future Direction of Use of Liquids For Electronics Reconfigurability For Sustainable Economy	Amit Kumar Baghel Pedro Pinho Nuno Borges Carvalho	University of Aveiro and Instituto de Telecomunicações
17:40-18:00	Study of Multipactor Effect in Bandpass Filters Implemented in Groove Gap Waveguide Technology	Angela Coves Alejandro Jorge-López José J. Vague Irene Asensio Ángel A. San Blas Mariano Baquero-Escudero Mariam Taroncher Ana Vidal, Vicente E. Boria	Dep. de Ingeniería de Comunicaciones, Instituto de Investigación en Ingeniería de Elche (I3E), Universidad Miguel Hernández de Elche, Spain Departamento de Comunicaciones-ITEAM, Universitat Politècnica de València, Spain
18:00-18:20	High Power Fully Canonical Triple Mode Filter for 5G Systems in S-Band	Cristóbal López-Montes José Ramón Montejo-Garai	Naval and Terrain Systems, Indra Sistemas S.A., Torrejón de Ardoz, Madrid, Spain Group of Applied Electromagnetics, Information Processing and Telecommunications Center, Universidad Politécnica de Madrid, Madrid, Spain.

Study of Multipactor Effect in Bandpass Filters Implemented in Groove Gap Waveguide Technology

Angela Coves*, Alejandro Jorge-López†, José J. Vague†, Irene Asensio†, Ángel A. San Blas*,
Mariano Baquero-Escudero†, Mariam Taroncher†, Ana Vidal†, Vicente E. Boria†
*Dep. Ing. Comunicaciones-I3E, Universidad Miguel Hernández de Elche, 03202 Elche, Spain, angela.coves@umh.es
†Departamento de Comunicaciones-ITEAM, Universitat Politècnica de València, 46022 Valencia, Spain

***Abstract*—In this work, it is studied the multipactor (MP) effect in bandpass filters implemented in groove gap waveguide (GGW) technology, which are based on rectangular cavities and inductive coupling irises. For the effective design of the considered GGW filter, an equivalent counterpart in standard rectangular waveguide (RW) technology has been first studied, using very efficient tools for computing its electrical response and MP threshold power levels P_{th}. Two prototypes of the GGW and RW bandpass filters, designed to operate at 17.5 GHz (for Ka-band satellite downlink applications) have been manufactured for validation and comparison purposes. Both of them are made of aluminium material, whose measured secondary electron emission properties have been considered in the prediction of MP threshold levels using available software tools. A good agreement between all simulated and experimental results of the MP effect has been achieved.**

***Index Terms*—filters, groove gap waveguide, multipactor.**

I. Introduction

Multipactor (MP) is a potentially harmful discharge effect that occurs inside microwave components operating under high-vacuum conditions. In such a case, electrons allocated inside the device can be accelerated by high-power electromagnetic (EM) fields and impact with the surrounding surfaces, yielding a resonant discharge inside the MP-affected component, which can cause signal harmonics, decrease the signal-to-noise ratio (SNR) and, eventually, cause physical damages [1].

On the other hand, a recently emerged technology for the practical implementation of high-frequency components relies upon the use of groove gap waveguides (GGWs) [2], in which periodic rows of pins are introduced in the GGW body, so the perfect metallic contact between the two parts (body and top cover) is not anymore needed. However, they may suffer MP breakdown within the tiny gaps between metallic surfaces (top cover and body), thus limiting their power-handling capabilities [3]. In this work, a comparison of the MP breakdown in a GGW filter and in its counterpart in standard RW technology is performed. Experimental results for both filter prototypes are compared and properly discussed.

II. Multipactor analysis of RW inductive filter

Inductively-coupled RW filters are based on the cascade connection of RWs (all with the same height, but with different width values), whose geometry (top-view) is shown in Fig. 1(a). For this work, a third-order RW filter, with a

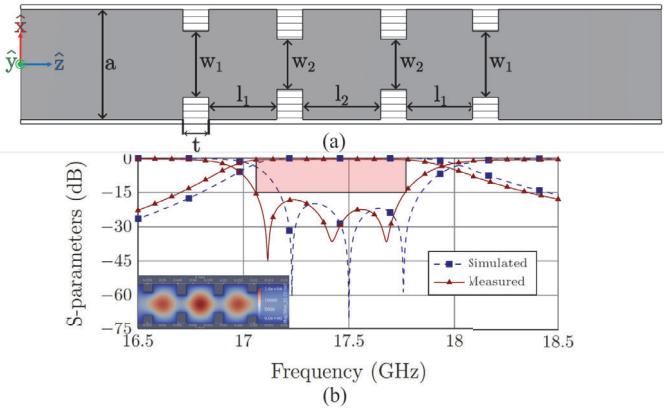

Fig. 1. (a) Geometry (top-view) and (b) simulated and measured electrical response of an inductive filter in RW technology (a= 12.95 mm, w_1= 7.73 mm, w_2= 5.86 mm, l_1= 8.05 mm, l_2= 9.18 mm and t= 3 mm, for a bandpass response of center frequency 17.5 GHz and relative bandwidth 3.85%). The height of the structure is 6.477 mm (for WR-51 ports) and 3 mm (for the optimal solution).

Chebyshev response centered at 17.5 GHz (Ka-band) with a relative bandwidth of 3.85% (around 675 MHz), has been designed using the automatic synthesis tool of FEST3D (now part of CST Studio Suite, Dassault Systèmes [4]). The resulting dimensions of such RW filter are included in the caption of Fig. 1, whereas its simulated electrical response (matching the required specifications) is shown in Fig. 1(b).

To feed the designed inductive filter, we have first considered a standard WR-51 RW (of size 12.954 mm $\times$ 6.477 mm), for which the MP breakdown power levels will be of several tens of kW (well beyond the maximum value in the available experimental facility [5], which is around 5 kW for the considered Ka-band frequency range). Thus, the height value must be properly reduced. We can see (Fig. 1(b)) that the maximum value of the electric field magnitude is located in the center of the second (central) cavity. Due to the particular geometry of inductive filters (invariant with height), the pattern for the electric field distribution is kept constant for any height value. Therefore, the same location for having a MP discharge can be considered in the iterative design process of the filter height. Thus, we will first compute the MP threshold power of a uniform section of the RW implementing the central cavity (P_{TH}), using a MP analysis tool based on the effective-electron model originally developed and validated in [6],

TABLE I
STANDARD AND MEASURED SEY DATA FOR ALUMINIUM (AL) MATERIAL.

Material	E_{max} (eV)	E_1 (eV)	δ_0	δ_{max}
Al (ECSS2020 [8])	276.000	17.000	0.800	2.920
Al (measured)	246.500	16.154	0.903	2.485

[7] (named as Numerical-RW in this article). Additionally, a simplified version of the previous tool (based on the analytical resolution of the effective electron trajectory) was developed and it has also been used for this work (called Analytical-RW from now on), which is extremely fast, and particularly suitable for the proposed iterative procedure. It is based on neglecting the influence of the magnetic field components of the RW fundamental mode, valid under non-relativistic velocities, which is the usual case in microwave hardware for satellite applications.

We can relate the P_{TH} value with the peak voltage level (V_{TH}) required for such a discharge:

$$V_{TH} = V_{1W} \sqrt{\frac{P_{TH}}{P_{1W}}} = V_{1W} \sqrt{P_{TH}} \qquad (1)$$

where V_{1W} is the peak voltage in the critical gap of the uniform RW (which is located at the waveguide center, where the electric field is maximum), for a mean power level of 1 W at the waveguide input port (P_{1W}= 1 W). However, we finally need to know the MP threshold power at the input port of the whole inductive filter (P_{FTH}), that will be lower than the previous one (P_{TH}) due to the voltage magnification effect originated in the resonant cavities of bandpass filters [9], being as follows:

$$P_{FTH} = P_{F1W} \left(\frac{V_{TH}}{V_{F1W}}\right)^2 = P_{TH} \left(\frac{V_{1W}}{V_{F1W}}\right)^2 \qquad (2)$$

where V_{F1W} is the value of the peak voltage in the middle of the central resonant cavity of the filter for a 1 W mean power level at the filter input port. It must be noted that the values of V_{1W} and V_{F1W} are also efficiently computed with the software tool FEST3D. Applying this procedure to our case, iteratively, an optimal value of 3 mm for the RW filter height is found after completing few simple steps.

Next, we have checked that the two efficient MP analysis tools used in this work (the Numerical-RW and the Analytical-RW ones) do also provide accurate results. For this purpose, we have first considered a uniform RW section of size 12.954 mm × 3 mm, made of aluminium material (whose standard SEY data, from [8] and compiled in Table I, are used). For validation of the P_{TH} values obtained for the cited RW, we have also used the well-known software tool SPARK3D (v. 2023, Dassault Systèmes). In order to get the results with SPARK3D, 10 000 initial electrons were homogeneously distributed within the uniform RW section, thus involving 24 hours for the complete simulation of MP effect at each frequency point. This extremely large computational effort is directly related to the very high order of the MP mode excited in the uniform RW (that SPARK3D has predicted to be

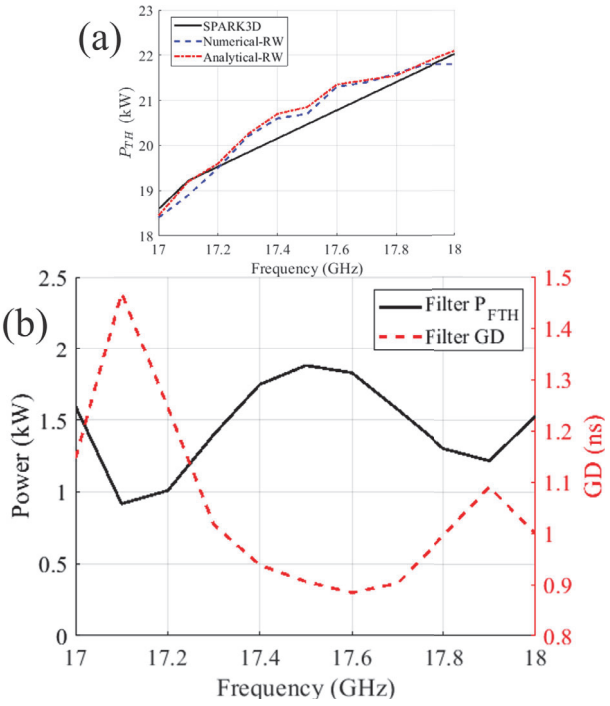

Fig. 2. (a) P_{TH} for the WR-51 RW with a height of 3 mm, computed with SPARK3D (solid line) and with the two efficient MP tools for RWs (Numerical-RW and Analytical-RW with dashed and dotted lines). (b) P_{TH} of the filter in WR-51 RW with a height of 3 mm (P_{FTH}, left-hand side scale), and filter group delay (GD, right-hand side scale), computed with the Analytical-RW tool (P_{TH} values) and FEST3D, respectively.

equal to 73), as it can be expected for a value of the frequency-gap product ($f \times d$) of 52.5 GHz × mm, considering the central frequency of 17.5 GHz. Using the two efficient tools for the MP effect analysis, properly configured as detailed next, we have also computed a very close value (of 71) for the order of the excited discharge mode. These results confirm that a large number of half-cycles of the sinusoidal excitation signal must be considered to reach reliable MP results. Thus, longer temporal simulation intervals will be involved, which discourages the use of very accurate (but less computationally efficient) commercial tools in this case. On the other hand, both the Numerical-RW and the Analytical-RW tools have computed the P_{TH} values in the uniform RW section following the same statistical approach. For each power value, the trajectories of 36 effective electrons, with initial phases of the driving electric field uniformly distributed between 0° and 360°, are computed. They are launched from the center of the RW, and from random positions between y= -1.5 mm and y= 1.5 mm (for the considered height of 3 mm). After 300 periods ($T = 1/f$), for all simulated trajectories, the average value of the final population of electrons (N) is used to determine (if such a value is above 1) that a MP discharge has occurred. It is important to note that the results obtained with the Analytical-RW tool were computed in just 2 minutes per frequency point, while those provided by the Numerical-RW approach took 55 minutes per frequency point. Fig. 2(a) shows

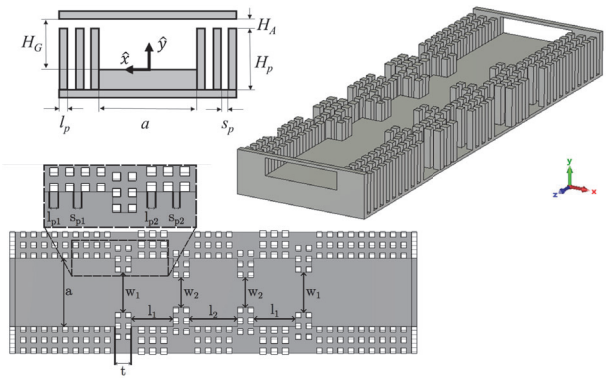

Fig. 3. 3-D view of the inductive bandpass filter in GGW technology and 2-D geometrical representation of each GGW.

the three sets of P_{TH} results for 11 points in the frequency range from 17 GHz to 18 GHz, that were obtained with an Intel(R) Xeon(R) computer at 2.10 GHz with 64 GB RAM. As can be seen, a very good agreement between all MP results is achieved.

Next, using the values of P_{TH} provided by the Analytical-RW tool (see Fig. 2(a)) in eq. (2), together with values for V_{1W} and V_{F1W} computed before, we have finally estimated the levels of P_{FTH} of the RW inductive filter (see Fig. 2(b)), which are entirely aligned with the electrical response of the designed RW filter (also represented in Fig. 2(b) through the group delay (GD) parameter). As can be seen, the minimum values of P_{FTH} are coincident with the peaks (maximums) of the filter GD (where the time-averaged stored energy (TASE) in the filter structure is also maximized) [10]. From results in Fig. 2(b), it is confirmed that the RW filter (of 3 mm height) is suitable for performing MP measurements in the selected facility. Finally, we have computed the value of P_{FTH} for the RW filter (at 17.5 GHz) using the accurate commercial tool SPARK3D, which predicts a value of 3093 W for P_{FTH} (higher than the maximum value at 17.5 GHz in Fig. 2(b), but still distant enough from the 5 kW limit of the experimental facility).

III. Multipactor analysis of GGW inductive filter

Once the RW inductive bandpass filter has been deeply studied, we will proceed with its practical implementation in GGW technology (see the 3-D view of the proposed topology in Fig. 3), and the corresponding MP analysis. For these purposes, CST Studio Suite [4] and the electrons tracking code SPARK3D will be used. To alleviate the corresponding computational burdens, we will rely on the available RW inductive solution as it is described next.

First, each RW (with the optimal height of 3 mm found in section II) of the inductive filter is directly replaced with its corresponding GGW counterpart (whose geometrical details are given in Fig. 3). Regarding the periodic bed of pins (of square cross-section with size l_p separated a distance equal to s_p, see Fig. 3), it has been properly designed for implementing the high-impedance surface of the GGW technology, thus

TABLE II
Optimized values for dimensions (all in mm) of the RW and GGW inductive filters.

Dimension	a	w_1	l_1	w_2	l_2	t
RW	12.95	7.73	8.05	5.86	9.18	3.00
GGW	12.95	7.71	7.89	5.80	9.07	3.00

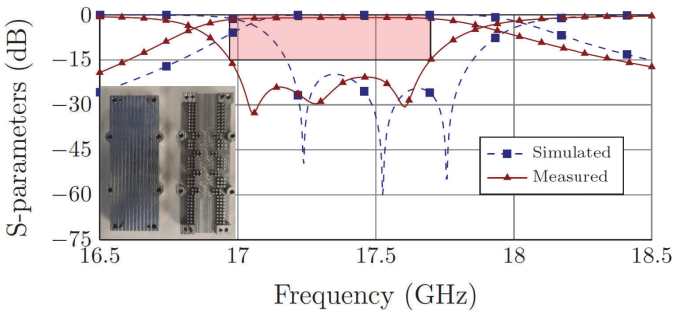

Fig. 4. Simulated and measured electrical response (S-parameters) of the GGW inductive filter (including the E-plane tapered transformers).

obtaining l_p= 1.02 mm and s_p= 0.96 mm for a nominal height value of H_p= 6.477 mm. Such a textured surface, together with the top metal lid, prevent any potential leakage of EM energy through the GGW lateral sides [11]. In this work, the zero-gap GGW realization (with $H_A \leqslant 20\,\mu$m) in Fig. 3 is used, which is very convenient to avoid undesired MP discharges. For the considered range of realistic values for H_A, and at frequencies in the operational bandwidth of the GGW filter (below 18 GHz), the frequency-gap product ($f \times d$) will always meet that $f \times d \leqslant 0.36\,\text{GHz} \times \text{mm}$. Based on the standard susceptibility charts for aluminium material [12], and for such low values of the $f \times d$ term, it can be noticed that no MP discharge (of any order) will ever occur. As a result, we can also replace RWs by real GGW realizations (with $H_A \leqslant 20\,\mu$m) without affecting the MP response of the inductive filter.

It is an optimal choice to use, as initial values for all dimensions of the GGW filter to be designed, those found for the RW case (whose data are compiled in the first row of Table II). Proceeding in this way, the entire design process of the inductive bandpass filter in zero-gap ($H_A = 0\,\mu$m) GGW technology is completed after few steps. All geometrical dimensions involved at the filter design stage are shown in Fig. 3, where it can be seen that most of pins are like those used before in the GGW body (i.e. with $l_{p1} = l_p = 1.02\,\text{mm}$ and $s_{p1} = s_p = 0.96\,\text{mm}$), whereas the lateral pins of the first and third filter cavities do have $l_{p2} = 1.2\,\text{mm}$ and $s_{p2} = 0.9\,\text{mm}$ to best fit the requested optimal value for the length of such two resonators. A satisfactory bandpass response, fully compliant with the filter specifications in terms of central frequency and bandwidth, is also achieved (see Fig. 4). These results also remain stable if some tiny air gaps were present (due to minor fabrication errors) above the metallic pins. The predicted value for the MP threshold power of the GGW filter is 3188 W, which is very close (slightly higher) to the result for the equivalent RW filter (of 3093 W, as stated in section II).

TABLE III
SIMULATED (SPARK3D) AND MEASURED RESULTS (MP THRESHOLD LEVELS) FOR RW AND GGW FILTERS AT 17.4 GHZ.

Model - Experiment	MP threshold (W)
RW simulation (ECSS2020 SEY)	3023.35
RW simulation (measured SEY)	3445.23
RW MP test	3424.50
GGW simulation (ECSS2020 SEY)	3163.98
GGW simulation (measured SEY)	3679.61
GGW MP test	3468.30

IV. EXPERIMENTAL RESULTS AND DISCUSSION

The two RW and GGW filters designed before (sections II and III) have been manufactured in aluminium, using an in-house computer numerical control (CNC) milling technique. As can be seen for the GGW filter case shown in Fig. 4, they consist of a body and a smooth top metal lid. In order to measure both filters, since their input and output ports have a height of 3 mm, E-plane tapered transformers to standard WR-51 RWs (with a height value of 6.477 mm) have been designed and built [13]. Comparisons between the simulated and measured results of the electrical response of the RW and GGW filter prototypes are shown in Fig. 1 and Fig. 4, respectively. There is a frequency shift of 170 MHz (below 1% in relative terms) between both GGW filter responses, which can be attributed to the mechanical tolerances (of 20 μm). Nevertheless, since the measured return loss levels are below 15 dB in the slightly shifted in-band responses, it will be possible to perform the MP study (analysis and, in particular, testing) of both filter units. In this case, such results will be obtained at the frequency of 17.4 GHz, where the pass-bands of the two fabricated prototypes are actually centered. The corresponding experimental SEY data have been obtained, from one metallic top lid of the filters, through measurements performed at the European High Power Space Materials Laboratory [5] (see Table I in section II).

For validation purposes, a MP test campaign (of both RW and GGW filter prototypes) was completed at the European High Power RF Space Laboratory [5]. As can be seen in Table III, the MP threshold simulated results (using the experimental SEY data) are remarkably similar to the corresponding measured data. It must be also noted that the MP experimental results are also very close for both technological realizations (RW and GGW) of the considered inductive filters.

V. CONCLUSION

In this work, a comparative study (based on theoretical and experimental results) of the MP effect for inductively coupled bandpass filters in RW and GGW technologies, is fully detailed. For that purpose, two filter units operating in the frequency range (17-18 GHz) planned for Ka-band satellite communications have been considered. For the effective design of the RW and GGW filters, very efficient modeling tools in RWs have been successfully applied. Then, more accurate results validating the MP response of the two given filter geometries, have been computed with Spark3D.

The measured MP results in both RW and GGW filters are very similar to those predicted by precise simulators incorporating the experimental SEY data, concluding that bandpass filters properly realized in the zero-gap GGW technology have very large MP threshold power levels, confirming the practical use of GGW filters in real space applications operating at the most challenging Ka-band frequency range.

ACKNOWLEDGMENT

This work has been funded by the Ministerio de Ciencia, Innovacion y Universidades (Spanish Government) through the Subprojects C41 and C43 of the R&D Projects PID2022-136590OB (under grant AEI/10.13039/501100011033/FEDER, UE) and TED2021-129196B (under grant 10.13039/501100011033/Unión Europea NextGenerationEU/PRTR), and through the Project RED2022-134657-T.

REFERENCES

[1] M. Jimenez, B. Gimeno, C. Miquel-Espanya, D. Raboso, S. Anza, C. Vicente, J. Gil, F. Pereira, A. Melcón, M. Taroncher, M. Reglero, and V.E. Boria, "Analysis of the electromagnetic radiation generated by a multipactor discharge occurring within a microwave passive component," *J. Phys. D, Appl. Phys.*, vol. 43, no. 39, Oct. 2010, Art. no. 395501.

[2] E. Rajo-Iglesias and P.-S. Kildal, "Groove gap waveguide: A rectangular waveguide between contactless metal plates enabled by parallel-plate cut-off," in *Proc. 4th Eur. Conf. Antennas Propag.*, Barcelona, Spain, Apr. 2010, pp. 1–4.

[3] J. Vague, I. Asensio, Á. Coves, Á. San Blas, M. Reglero, A. Vidal, D. Raboso, M. Baquero-Escudero, and V.E. Boria, "Study of the multipactor effect in groove gap waveguide technology," *IEEE Trans. Microw. Theory Tech.*, vol. 70, no. 5, pp. 2566–2578, May 2022.

[4] CST Microwave Studio. [Online]. Available: https://www.3ds.com/products/simulia/cst-studio-suite

[5] European Space Agency and Val Space Consortium-European Space Agency High-Power Laboratories, Valencia, Spain. [Online]. Available: www.val-space.com

[6] A. Berenguer, Á. Coves, F. Mesa, E. Bronchalo, and B. Gimeno, "Analysis of multipactor effect in a partially dielectric-loaded rectangular waveguide," *IEEE Trans. Plasma Sci.*, vol. 47, no. 1, pp. 259–265, Jan. 2019.

[7] A. Berenguer, Á. Coves, B. Gimeno, E. Bronchalo, and V.E. Boria, "Experimental study of the multipactor effect in a partially dielectric-loaded rectangular waveguide," *IEEE Microw. Wireless Compon. Lett.*, vol. 29, no. 9, pp. 595–597, Sep. 2019.

[8] *Multipacting Design and Test*, document ECSS-E-ST-20-01C, European Cooperation for Space Standarization (ECSS), ESA-ESTEC, ESA Publication Division, Amsterdam, The Netherlands, Jun. 2020.

[9] R. J. Cameron, C. M. Kudsia, and R. R. Mansour, *Microwave Filters for Communication Systems: Fundamentals, Design, and Applications*, 2nd ed. Hoboken, NJ, USA: Wiley, 2018.

[10] P. Gonzalez, C. Alcaide, R. Cervera, M. Rodríguez, O. Monerris, J. Petit, A. Rodríguez, A. Vidal, J. Vague, J.V. Morro, P. Soto, and V.E. Boria, "Multipactor threshold estimation techniques based on circuit models electromagnetic fields and particle simulators", *IEEE J. Microw.*, vol. 2, no. 1, pp. 57-77, Jan. 2022.

[11] P.-S. Kildal, E. Alfonso, A. Valero-Nogueira, and E. Rajo-Iglesias, "Local metamaterial-based waveguides in gaps between parallel metal plates," *IEEE Antennas Wireless Propag. Lett.*, vol. 8, pp. 84–87, 2009.

[12] A. Woode and J. Petit, "Diagnostic investigations into the multipactor effect, susceptibility zone measurements and parameters affecting a discharge," ESA/ESTEC, Noordwijk, The Netherlands, Work. Paper 1556, Nov. 1989.

[13] S. Cogollos, J. Vague, V.E. Boria, and J. D. Martínez, "Novel planar and waveguide implementations of impedance matching networks based on tapered lines using generalized superellipses," *IEEE Trans. Microw. Theory Techn.*, vol. 66, no. 4, pp. 1874–1884, Apr. 2018.